

Temperature Dependences of Torque Generation and Membrane Voltage in the Bacterial Flagellar Motor

Yuichi Inoue,[†] Matthew A. B. Baker,[‡] Hajime Fukuoka,[†] Hiroto Takahashi,[†] Richard M. Berry,[‡] and Akihiko Ishijima^{†*}

[†]Institute of Multidisciplinary Research for Advanced Materials, Tohoku University, Aoba-ku, Sendai, Japan; and [‡]Clarendon Laboratory, Oxford University, Oxford, United Kingdom

ABSTRACT In their natural habitats bacteria are frequently exposed to sudden changes in temperature that have been shown to affect their swimming. With our believed to be new methods of rapid temperature control for single-molecule microscopy, we measured here the thermal response of the Na⁺-driven chimeric motor expressed in *Escherichia coli* cells. Motor torque at low load (0.35 μm bead) increased linearly with temperature, twofold between 15°C and 40°C, and torque at high load (1.0 μm bead) was independent of temperature, as reported for the H⁺-driven motor. Single cell membrane voltages were measured by fluorescence imaging and these were almost constant (~ 120 mV) over the same temperature range. When the motor was heated above 40°C for 1–2 min the torque at high load dropped reversibly, recovering upon cooling below 40°C. This response was repeatable over as many as 10 heating cycles. Both increases and decreases in torque showed stepwise torque changes with unitary size ~ 150 pN nm, close to the torque of a single stator at room temperature (~ 180 pN nm), indicating that dynamic stator dissociation occurs at high temperature, with rebinding upon cooling. Our results suggest that the temperature-dependent assembly of stators is a general feature of flagellar motors.

INTRODUCTION

The bacterial flagellar motor is a rotary machine that drives swimming in many species of bacteria (1). The motor is powered by the flow of ions driven by an inward directed electrochemical gradient across the cytoplasmic membrane. The torque-generating unit in the motor is called a stator, which is composed of two proteins: MotA and MotB in the H⁺-driven motor in *Escherichia coli*, or PomA and PomB in the Na⁺-driven motor in *Vibrio alginolyticus*. The chimeric motor whose stator contains PomA and a chimeric protein PotB can be expressed in *E. coli* cells as a Na⁺-driven motor (2). Because this chimeric motor is suited for manipulation of energy input as well as various mutations, it is ideal for the study of the molecular mechanism of energy transduction from chemical energy into mechanical work. Using the chimeric motor, the number of stators in one motor is reported as ~ 11 (3) and angular step during a rotation is found to be ~ 26 steps per one revolution (4).

Motility of the flagellar motor is characterized by plotting a torque-speed (T-S) curve, a standard test for the theoretical models of motor function. For H⁺-driven motors in *E. coli* cells, the effect of temperature on the T-S curve had been measured in the temperature ranges 16–23°C (5) and 8–37°C (6), in which speed at low load strongly depends on temperature, whereas speed at high load hardly changes with temperature. However, because these measurements were performed with each individual motor at constant tem-

perature, the transient response of the bacterial flagellar motor to rapid temperature changes is not well characterized and responses to temperatures $>37^\circ\text{C}$ have not been measured. For Na⁺-driven motors, the T-S curve has been measured only at room temperature (7).

Several residues in the component proteins of the flagellar motor have been identified in temperature-sensitive (TS) mutants (8,9). For PomA in the Na⁺-driven motor of *Vibrio*, point mutations in particular residues in a cytoplasmic loop abolished swimming of the cell body at 42°C, whereas the wild-type (WT) motor showed normal swimming (8). For rotor protein FliG in *Salmonella enterica* serovar Typhimurium, motors with point mutations in rotor proteins (FliG, FliM, and FliN) were temperature sensitive (9). In both reports, some TS mutants showed a temperature-sensitive response in swimming rate, in which they did not swim at high temperature but recovered swimming when the temperature was restored to room temperature. Because it is proposed that electrostatic interaction between the cytoplasmic loop of PomA and the surface of FliG is essential for the mechanism of torque generation (10), thermal response of the TS mutant may be related to the mechanism of torque generation, as well as that of the thermal tolerance.

The membrane voltage of bacteria is the primary component of the ion motive force that drives the rotation of the flagellar motor. Membrane voltage in *E. coli* cells was recently measured by single-cell imaging using the Nernstian fluorescent dye, tetramethyl rhodamine methyl ester (TMRM) (11). The membrane voltage increased linearly with increasing external pH from 5.0 to 7.0, and was independent of the external Na⁺ concentration. Stator stability in the motor depends on ion-motive force (1,4,12,13),

Submitted August 7, 2013, and accepted for publication September 23, 2013.

*Correspondence: ishijima@tagen.tohoku.ac.jp

Editor: Kazuhiro Oiwa.

© 2013 by the Biophysical Society
0006-3495/13/12/2801/10 \$2.00



however it is not known how membrane voltage depends on temperature, and therefore whether or not it might be a factor influencing torque in motor thermal responses.

We previously developed new methods for rapid temperature control in single-molecule measurements with high numerical aperture objective lenses (14). Here, we used these methods to measure the responses of both torque in single Na^+ -driven chimeric motors and membrane voltage in single *E. coli* cells expressing chimeric motors. We found that membrane voltage remained close to -120 mV between 5°C and 40°C . Torque generated by chimeric motors between 15°C and 40°C was nonhysteretic, as in H^+ -driven motors (5,6). However, transient heating over 40°C induced a hysteretic response: reduction in torque at high temperature and recovery upon restoring temperature, similar to the temperature response of swimming speed in the TS mutants (8,9). During hysteresis we observed stepwise torque changes, with up to a maximum of 13 different torque levels.

MATERIALS AND METHODS

Bacteria and cultures

Chimeric motors with or without PomA mutation were expressed in *E. coli* strain JHC36 ($\Delta cheY$, $fliC^{sticky}$, $\Delta pilA$, $\Delta motAmotB$) with a plasmids pTH200 (PomA, PotB), pTH201 (PomA-R88A, PotB), or pTH202 (PomA-R232E, PotB), inducible by isopropyl- β -D-thiogalactopyranoside (IPTG), as previously (15). H^+ -driven motors were expressed in *E. coli* strain JHC36 with a plasmid pTH2300 (MotA, MotB) (16) inducible by IPTG. Cells were grown from frozen stocks with shaking in T-broth (1% Bacto tryptone, 0.5% NaCl) containing $25 \mu\text{g/ml}$ chloramphenicol and 0.05 mM IPTG at 31°C for 5 h.

Temperature control

Temperature of motors on a microscope with an oil-immersion objective (Plan Apo $\times 100$, numerical aperture 1.4, Olympus, Tokyo, Japan) was controlled by a fluid flow chip on the sample as previously (14,17). Temperature in a range of 5 – 50°C was controlled rapidly ($\sim 20^\circ\text{C}$ in 2 min) and repeatedly during a single motor measurement of the motors. For the fluid chip method, precise stable control within $\pm 1^\circ\text{C}$ is difficult to achieve due to the small thermal capacity in comparison with the varied heat of the fluid flowing through the chip. In particular, the remaining cold (or hot) water in the temperature-controller tubing produces a transient temperature change after changing the source of the flow (see Figs. 2 and 3, arrows). Temperature in single cellular measurement of membrane voltage was controlled by a ring-shaped Peltier collar attached to the objective (14).

Speed and torque measurements

Polystyrene beads ($1.053 \pm 0.010 \mu\text{m}$, $0.771 \pm 0.025 \mu\text{m}$, $0.548 \pm 0.016 \mu\text{m}$, and $0.356 \pm 0.014 \mu\text{m}$ diameter, Polyscience, Warrington, PA) were attached to truncated flagella and their position was measured with back-focal-plane interferometry as previously (15). Rotational speed was obtained from the largest peak in the power spectra of the bead position as described elsewhere (3). Due to thermal drift of the stage, speed calculation by fast Fourier transform sometimes failed, especially for smaller beads. Therefore, calculated speed was not always continuous (see Fig. 3 a). Torque was calculated as previously (15) with some modifications. In

short, torque generated by the motor was expressed as, $M = (f_b + f_f)\omega$, where f_b and f_f are rotational frictional drag coefficients of the bead and the filament stub and ω is angular velocity. The rotational frictional drag coefficients of the filament stub, f_f , was $0.127 \text{ pN nm s/rad}$ at 23°C , and was used after correcting the effect of sample temperature measured using a thermocouple as previously (14).

Analysis of the torque steps

Time course of the motor torque with a high load ($1.0 \mu\text{m}$ bead) was analyzed to find the steps in the significant torque change as $>2 \text{ pN nm/s}$. Analysis of the step finding was performed as previously (4,18) using a constant threshold of $Q = 10$, defined as $Q^2 = (x_1 - x_2)^2 / [(var_x/n_x) + (var_y/n_y)]$ where x_i , var_x , and n_x are the mean angle, the variance, and the number of points in an interval, respectively, and $i = 1$ and $i = 2$ indicate intervals immediately before and after a step.

Rotation of tethered cells under temperature control

A cultured solution of *E. coli* strains was applied to the sample chamber for 5 min to adsorb flagella of *E. coli* cells on to the glass slide. After perfusion with motility buffer (10 mM potassium phosphate, 85 mM NaCl, and 0.1 mM ethylenediaminetetraacetic acid, pH 7.0), rotation of *E. coli* cells was observed using an inverted microscope (IX70, Olympus, Tokyo, Japan) with a phase-contrast objective (UPlanFI $\times 40$, NA 0.75, Olympus, Tokyo, Japan). Using a fluid flow chip with hot water, sample temperature was risen with a slow rate of 0.02 – 0.50°C/s , until *E. coli* cells stop their rotation. For the simultaneous recording of temperature with a phase-contrast image of *E. coli* cells by a charge-coupled device camera (WAT100N, Watec, Yamagata, Japan), a display of the thermometer (HA-200E, Anritsu, Kanagawa, Japan) was imaged using a digital camera (F-30, Fujifilm, Tokyo, Japan) to combine with a screen separation device (MTQC-14, Mother tool, Nagano, Japan) in a picture-in-picture mode.

Measurement of membrane voltage

Single cellular measurement of membrane voltage was performed using the Nernstian fluorescent dye, TMRM as previously (11) with some modifications (Method S2 in the Supporting Material). Full details of the fluorescent measurement and the calculation of the membrane voltage are described in the Supporting Material.

RESULTS

Motor response under temperature control at high load

Rotational speed measurement of a single chimeric motor under temperature control was performed to examine thermal response of the chimeric motor, as illustrated in Fig. 1. Fig. 2 shows a typical result at high load using a $1.0 \mu\text{m}$ -diameter bead attached to a filament stub. Arrows (Fig. 2, top) indicate: (arrow 1) commencing cooling to $\sim 15^\circ\text{C}$ by starting the flow of cold water, (arrow 2) stopping cooling by stopping the flow, (arrow 3) restarting the flow with cold water at the source switched to hot water, (arrow 4) temporary cooling due to the transient flow of the remaining cold water in the temperature-controller tubing, and (arrow 5) commencing heating to $\sim 35^\circ\text{C}$ with hot water

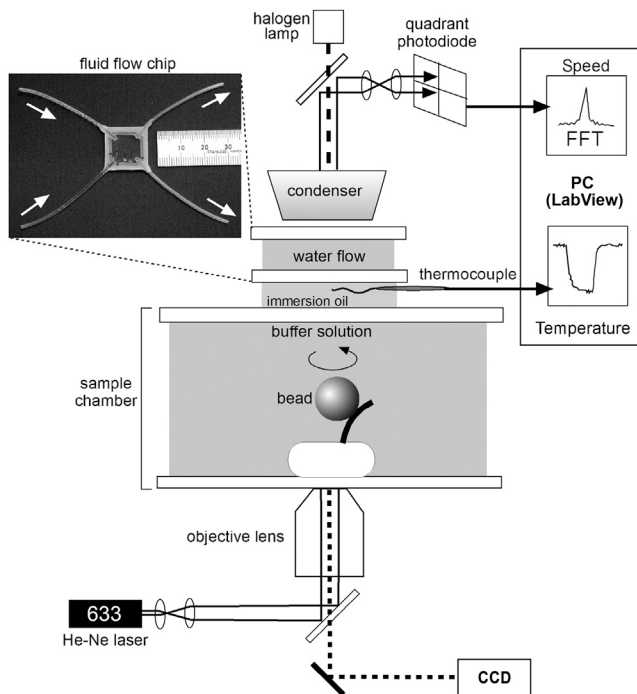


FIGURE 1 Schematic of measurement of motor rotation under temperature control. An *E. coli* cell was immobilized on the glass surface of a sample chamber and a bead was attached to its flagellar filament stub. The bead position was measured with back-focal-plane interferometry as previously (15). The temperature controller fluid flow chip was placed in close thermal contact with the sample chamber via immersion oil and temperature was monitored using a thermocouple as previously (14).

flow. The temperature change between 15°C and 35°C was accompanied by speed change between ~60 Hz and ~100 Hz (Fig. 2 A, middle). A plot of the speed with temperature shows a linear relationship between speed and temperature (Fig. 2 B, left). Torque, calculated from speed and temperature accounting for the temperature dependence of viscosity and its effect on the viscous drag coefficient of the bead (Materials and Methods), varied little from ~2000 pN nm during the temperature change (Fig. 2 A, bottom; Fig. 2 B, right), indicating that motor torque is insensitive to temperature at high load as previously reported for H⁺-driven motors (5,6).

Motor response under temperature control at low load

Fig. 3 shows a typical result at low load using a 0.36 μm-diameter bead. Following cooling and heating as in the experiment of Fig. 2 A (arrows 1–5), the motor was further heated to ~40°C by adding hot water at the temperature-controller source (Fig. 3 A, top, arrow 6 and arrow 7). In contrast to the constant torque measured at high load (Fig. 2), both speed (Fig. 3 A, middle; Fig. 3 B, left) and torque (Fig. 3 A, bottom; Fig. 3 B, right) at low load increased approximately linearly with temperature. The

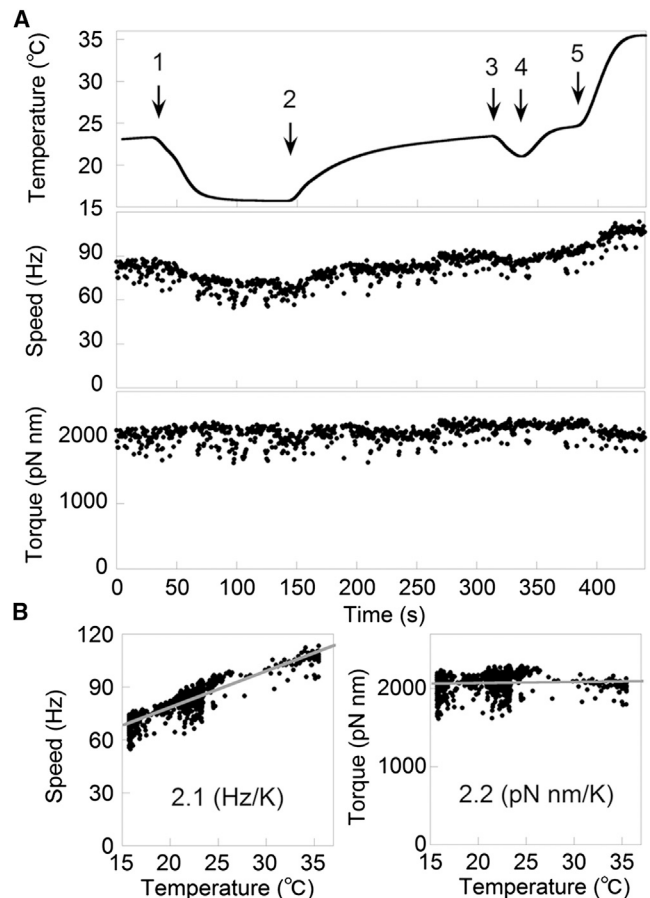


FIGURE 2 Speed measurement at high load. Typical temperature response of a motor at high load (1.0 μm-diameter bead), 15–35°C. (A) Time courses of temperature (top), speed of the chimeric motor (middle), and torque (calculated as described in Materials and Methods, bottom). Arrows indicate: (arrow 1) commencing cooling to ~15°C by starting the flow of cold water, (arrow 2) stopping cooling by stopping the flow, (arrow 3) restarting the flow with cold water at the source switched to hot water, (arrow 4) temporary cooling due to the transient flow of the remaining cold water in the temperature-controller tubing, and (arrow 5) commencing heating to ~35°C with hot water flow. (B) Relationships between speed and temperature (left) and between torque and temperature (right) from data of A. Gray lines are linear fits.

linear relationships between speed and temperature extended to ~40°C.

T-S curve up to 40°C

In the temperature range 10–40°C, rotational speed of the chimeric motor was nonhysteretic (Figs. 2 and 3). Motor torque measured for 15 cells under 4 load conditions between 10°C and 40°C is plotted versus speed in Fig. 4 A. Speed at low load (0.35 μm, 0.55 μm beads) depends much more on temperature than speed at high load (0.77 μm, 1.0 μm). Data in the three typical temperature ranges, 15 ± 1°C, 23 ± 1°C, and 40 ± 1°C, were selected and averaged to characterize the temperature-dependence

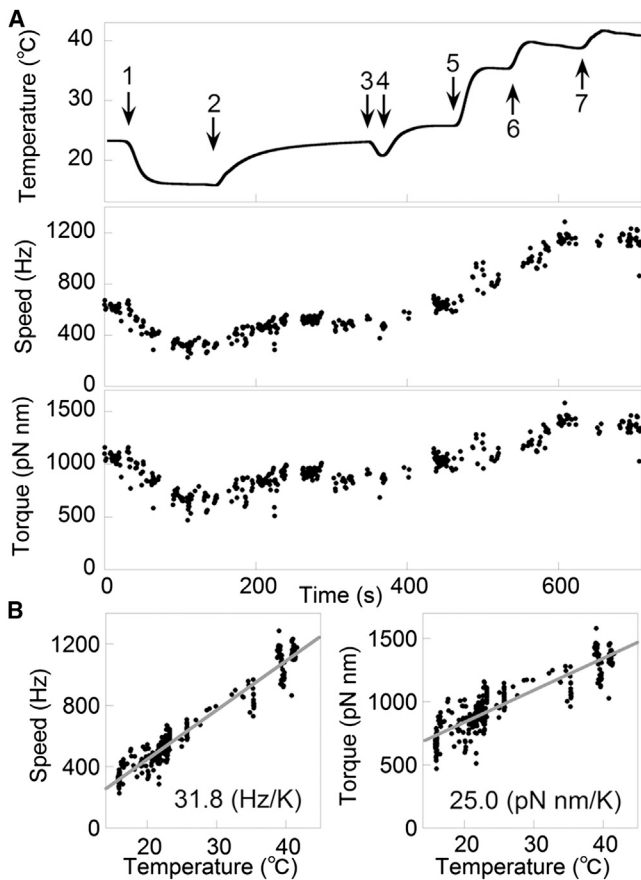


FIGURE 3 Speed measurement at low load. Typical temperature response of a motor at low load (0.36 μm -diameter bead), 15–40°C. (A) Time courses of temperature (top), speed of the chimeric motor (middle), and torque (calculated as described in Materials and Methods, bottom). Arrows 1–5 indicate temperature changes as in Fig. 2 A and additional arrows 6 and 7 indicate further heating by adding hot water at the source. (B) Relationships between speed and temperature (left) and between torque and temperature (right) from data of A. Gray lines are linear fits.

(Fig. 4 B). The effect of cooling from room temperature on the T-S curve of the chimeric motor was similar to that reported for the H^+ -driven motor (5), and the trend extended to $\sim 40^\circ\text{C}$ in the T-S curve of the chimeric motor. Solid lines in Fig. 4 B show fits to the T-S curves for 15°C, 23°C, and 40°C with a kinetic model (19). The T-S curve at 23°C was fitted with kinetic parameters shown in Fig. S3 (black line for 23°C). T-S curves for 15°C and 40°C could be fitted with a change in a single parameter k_0 (0.55-fold for 15°C and 2.5-fold for 40°C, solid lines in Fig. 4 B, see Discussion).

Measurement of membrane voltage at 5–40°C

To measure membrane voltage (V_m) using the ratiometric cationic dye TMRM, we first calculated the internal and external concentrations of the dye following the method of Lo et al. (11) with modifications (see the Supporting Material for details). For each image, a cell was identified as all continuously linked pixels brighter than T_{thresh} (one stan-

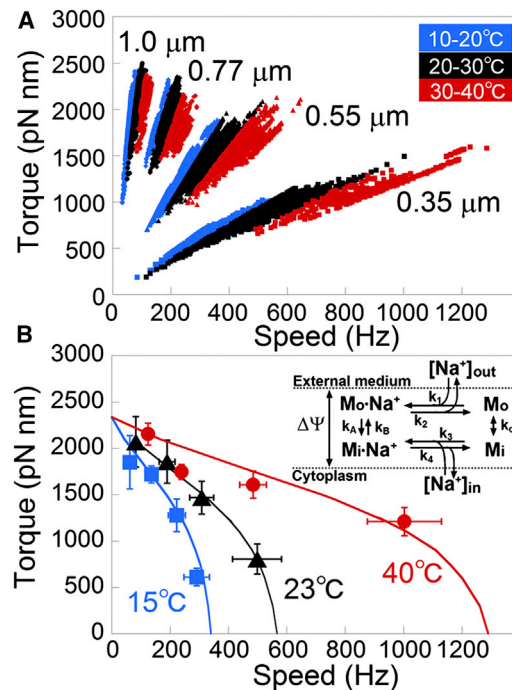


FIGURE 4 T-S curves at 15–40°C. (A) Relationship between speed and torque of the chimeric motor measured with 1.0 μm (circles), 0.77 μm (diamonds), 0.55 μm (triangles), and 0.35 μm diameter beads (squares). Data were taken from 15 motors, each measured in the temperature ranges shown in Figs. 2 and 3. (B) Averaged data from A showing the effect of temperature on the T-S curve. Data were averaged over short temperature ranges for low temperature ($15 \pm 1^\circ\text{C}$, blue squares), room temperature ($23 \pm 1^\circ\text{C}$, black triangles), and high temperature ($40 \pm 1^\circ\text{C}$, red circles). Solid lines for 15°C, 23°C, and 40°C show the fit to the kinetic model (inset, see Discussion). To see this figure in color, go online.

dard deviation above the image mean—cells are typically brighter than the background). Fig. 5 A shows a pixel intensity histogram for a typical image, with a large peak corresponding to the background and a long tail corresponding to the brighter cell. The mean external brightness ($T_{\text{background}}$), the median brightness of the cell (T_{median}), and the mean brightness of all pixels brighter than T_{median} (T_{cell}) are indicated on the histogram. The internal fluorescent intensity was defined as $M_{\text{live}} = T_{\text{cell}} - T_{\text{background}}$. This definition includes only the central part of the cell, making it insensitive to cell size and edge effects (20). External fluorescence intensity (M_{absent}) was determined by fitting images with no cell in the field of view, taken with a range of exposure times (0.001–0.5 s). These internal and external fluorescent intensities were used to estimate the corresponding dye concentrations using the linear model described in Method S1 in the Supporting Material. We extended the method of Lo et al. (11) to account for any membrane-bound dye, as described (Method S2). The intracellular fluorescent intensity was measured again (M_{CCCP}) ~ 30 min after application of 100 μM carbonyl cyanide 3-chlorophenylhydrazone (CCCP), which dissipated the membrane voltage and thus matched the intracellular and

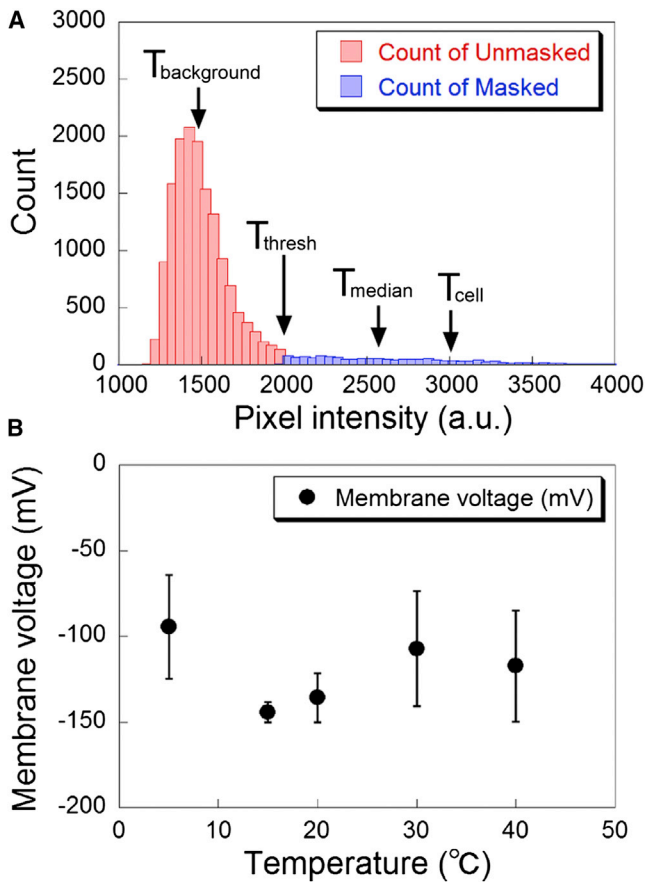


FIGURE 5 Measurement of membrane voltage. (A) Histogram of the fluorescence intensity of a cell. Histogram pixel intensity across a single image, with the histogram of the pixels in the interior of the cell shown in blue and the histogram of the pixels outside the cell mask shown in red using method adapted from Lo et. al. (11). First, a cell mask is generated by finding the largest area of continuously linked pixels that had intensity at least one standard deviation greater than the mean (T_{thresh}). To calculate the fluorescence intensity of the cell (M_{live}), we measured the fluorescence contribution from the cell, that is, the difference between the cell brightness (T_{cell}), and the camera background ($T_{background}$). To account for variance introduced from variation in cell size or edge effects, we calculated the mean over the internal section of the cell (T_{cell}), defined as the pixels brighter than the median cell pixel intensity (T_{median}), as per Lo et. al. (20). To measure $T_{background}$, the mean over all pixels outside the mask was calculated. All of T_{thresh} , T_{cell} , $T_{background}$, and T_{median} are indicated by arrows. The intensity measurement, M_{live} , for this cell is 1692. These fluorescence measurements are subsequently interconverted into internal and external concentrations of dye using the linear model detailed in Method S1 in the Supporting Material, adapted from the method of Lo et. al. (11). (B) Membrane voltage measured for 5–40°C. At constant temperature (5, 15, 20, 30, or 40°C), the fluorescence intensity of cells was measured. Number of cells was 159, 46, 102, 31, or 158 for 5, 15, 22, 30, or 40°C, respectively. Membrane voltage was calculated from M_{live} , M_{absent} , and M_{CCCP} using the extended linear model as summarized in the text (Method S2 in the Supporting Material). To see this figure in color, go online.

extracellular dye concentrations. Subtracting M_{CCCP} from M_{live} corrected for the fluorescence contribution from any membrane-bound dye.

31–159 cells were imaged under constant temperature (5, 15, 20, 30, or 40°C) and their membrane voltages estimated from M_{live} , M_{absent} , and M_{CCCP} using an extended linear model (Method S2). Temperature-dependence of TMRM fluorescence, $-2\%/^{\circ}\text{C}$, was corrected by taking the background measurement, M_{absent} , at each temperature. Fig. 5 B shows the average membrane voltage measured between 5°C and 40°C, which was constant within the limits of experimental error (-120 ± 23 mV) throughout the temperature range.

Motor response to transient heating over 40°C

We found that the thermal response of the chimeric motor showed hysteresis above 40°C. Fig. 6 A shows temperature, speed, and torque at high load (1.0 μm -diameter bead) in four cycles of transient heating above 40°C. In contrast to the constant torque between 15°C and 40°C (Fig. 2), both speed and torque dropped toward zero after heating above 40°C for 1–2 min (red in Fig. 6). When the temperature

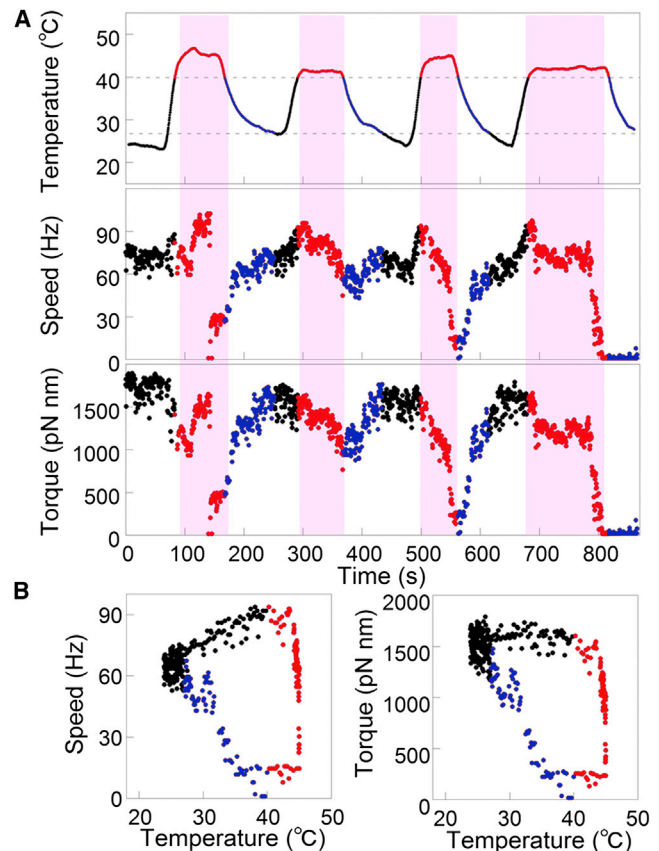


FIGURE 6 Transient heating over 40°C. (A) Bead assay at high load (1.0 μm -diameter bead) for 4 cycles of heating to 40–50°C for 1–2 min. Time course of temperature (top), rotational speed (middle), and calculated torque (bottom). Pink bar shows heating over 40°C and the corresponding data are shown in red. Data during restoration of temperature from 40°C to 27°C are shown in blue. (B) Relationships between speed and temperature (left) and between torque and temperature (right) from the 3rd heating cycle (500–650 s) in A. Data colored as in A. To see this figure in color, go online.

was restored to room temperature, speed and torque recovered to original levels (blue in Fig. 6). The time constant estimated from single exponential fits to the recovery torque (56 ± 5 s) was slower than that of the restoring temperature (35 ± 0.6 s), indicating that the response of the motor is distinct from any viscosity-related temperature effects. We observed several cycles of loss and recovery of motor torque with transient heating, indicating that the motor response is a reversible process. How far the cell is heated above 40°C , and the duration of the heating, may relate to how reversible this torque change is. Fig. 6 B shows speed (left) and torque (right) plotted against temperature in the 3rd cycle in Fig. 6 A (500–650 s). In contrast to the temperature-dependent linear changes of speed and torque at $15\text{--}40^\circ\text{C}$ (Fig. 2 B), both speed and torque showed a hysteresis loop as the temperature is increased above 40°C (Fig. 6 B).

Stepwise torque change induced by heating

Fig. 7 shows selected traces from the torque transients induced by overheating. Torque changed in discrete steps

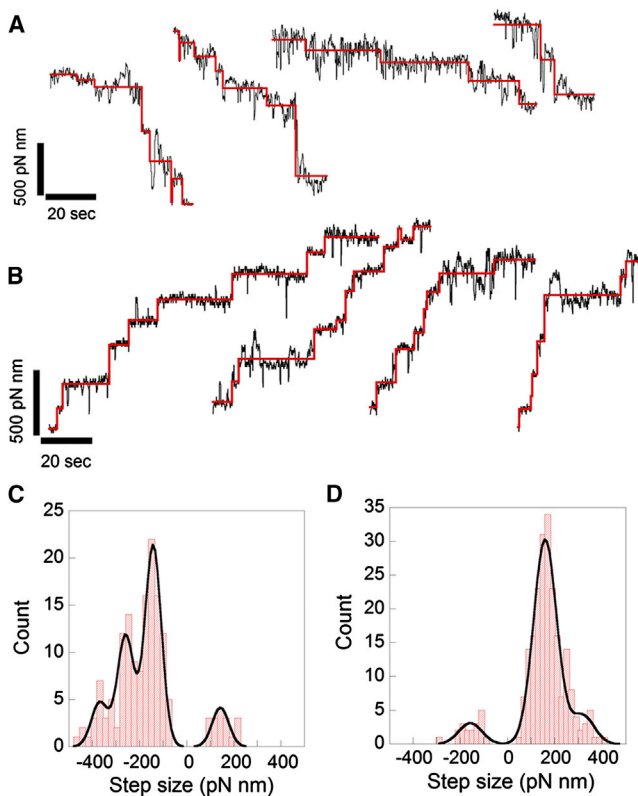


FIGURE 7 Stepwise torque change induced by heating over 40°C . (A) Decremental torque steps induced by heating over 40°C . (B) Recovery torque steps when reducing temperature after heating. Solid lines in A and B show steps detected by a step-finding algorithm. (C and D) Histograms of step sizes from 30 traces as shown in A and B, respectively, measured over 1–12 heating cycles per motor. Solid lines are multiple Gaussian fits. The highest peaks are at -143 ± 35 in C and 158 ± 49 pN nm in D. To see this figure in color, go online.

in both falling (Fig. 7 A) and recovery (Fig. 7 B) phases. Solid lines in Fig. 7, A and B, show the steps detected by a step-finding algorithm (4,18). Histograms of the detected step size for the falling and recovery phases are shown in Fig. 7, C and D, respectively. Main peaks determined by fitting multiple Gaussian peaks to the histograms were -143 ± 35 and 158 ± 49 pN nm for Fig. 7, C and D, respectively. These results suggest that torque changes in a stepwise manner with a unitary step size of ~ 150 pN nm for both the falling and recovery phases.

Reproducibility of the torque change over a number of heating cycles ($40\text{--}50^\circ\text{C}$ for 1–2 min) was examined by plotting absolute values of mean step sizes of each trace against the cycle number (Fig. 8 A). The mean step size, $130\text{--}230$ pN nm, did not change significantly over 12 cycles, but was reduced to ~ 100 pN nm for the few measurements at the 13th, 14th, and 15th cycles. Fig. 8 B shows the maximum torque determined by the step-finder for each trace. The maximum torques measured for heating cycles 1–12 were $1400\text{--}2300$ pN nm (black circles) decreasing to ~ 1000 pN

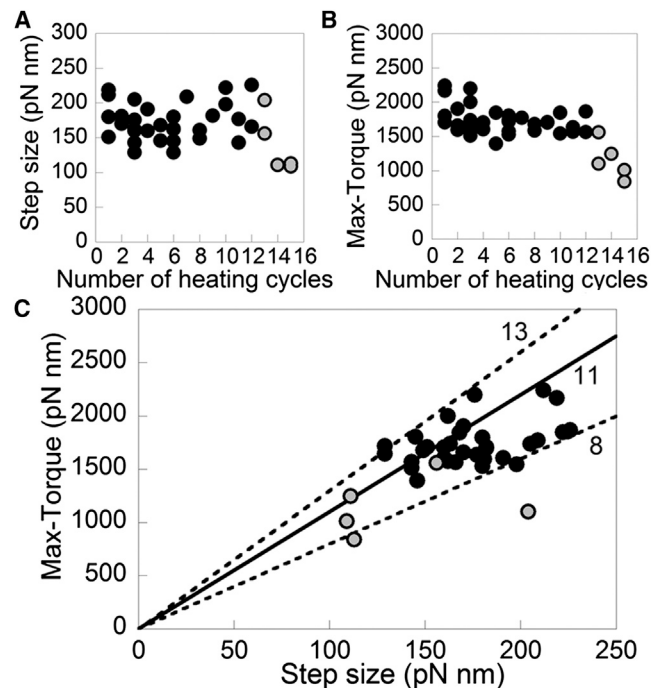


FIGURE 8 Thermal tolerance of the chimeric motor to repeated heating cycles. (A) Mean step size in rising and falling torque transients plotted against cycle number (1st–12th cycles: black circles, 13th–15th cycles: gray open circles). Mean step size was calculated for each torque transient that showed >4 steps of the type illustrated by solid lines in Fig. 7, A and B. To correct for multiple unresolved fast individual steps, all found steps larger than twice the mean over all steps were discarded, and the remaining steps were used to recalculate the mean. (B) Maximum torque level in each cycle, determined by the step-finder, plotted against cycle number (1st–12th cycles: black circles, 13th–15th cycles: gray open circles). (C) Relationship between the step size in A and the maximum torque in B. Lines corresponding to fixed ratios (8,11,13) suggests the number of the steps in each torque trace, and thus the total number of stators.

nm for cycles 13–15 (*gray open circles*). The relationship between the average step size and maximum torque level for each trace is plotted in Fig. 8 C, with different integer ratios indicated by lines. For heating cycles 1–12 (*black circles*) ratios fell in the range of 8–13, consistent with the expected maximum number of stators in a motor (3). Even for the heating cycles 13–15 (*gray open circles*) the ratio did not exceed 13. These results indicate that torque transients in cycles 1–12 are due to changes in the number of stators, with each stator generating ~150 pN nm, whereas during cycles 13–15 there is a reduction of the unitary torque per stator.

Thermal response of PomA mutants and H⁺-driven motor

We have reported previously that point mutations in PomA at conserved arginines (PomA-R88A and PomA-R232E) reduced both the swimming speed in solution and the motor torque as measured with the bead assay (15). Fig. 9 shows the temperature response of these mutants. Both show loss of torque at elevated temperatures: PomA-R88A showed reversible torque reduction below 40°C (Fig. 9 A); PomA-R232E showed irreversible torque reduction at ~30°C (Fig. 9 B). These results show that both mutants are more sensitive to temperature than the original motor. On the other hand, the WT H⁺-driven motor (MotA/MotB) showed a similar torque response to the chimeric motor (PomA/PotB), with reversible torque reduction at >40°C (Fig. 9 C). Stepwise changes in torque could be detected by the step-finder for both H⁺-driven motor (Fig. S4 in the Supporting Material) and the two mutants (Fig. S5).

We defined the nonpermissive temperature as the lowest temperature at which no rotation of the motor was ever observed during slow temperature increases of <1.0°C/s. The nonpermissive temperatures observed in the tethered cell experiment were 52.0 ± 0.6°C, 43.3 ± 1.1°C, 36.7 ± 0.4°C, and 58.2 ± 2.6°C for PomA, PomA-R88A, PomA-R232E, and H⁺-driven motor, respectively (Fig. 9 D), confirming that the PomA mutants are more sensitive to heating than the original motor and WT motor.

DISCUSSION

T-S curve at 10–40°C

Thermal responses up to 40°C were nonhysteretic: the membrane voltage was almost constant at –120 mV, and motor speed linearly changed with temperature, giving similar temperature dependence of the T-S curve to that reported for WT H⁺-driven motors (5), suggesting that H⁺- and Na⁺-driven motors have the same mechanism of thermal response in torque generation. Using a simple kinetic model, Iwazawa and co-workers explained the effect of temperature on the T-S relationship of H⁺-driven motors (19). T-S curves

of Na⁺-driven motors at room temperature were fitted with this kinetic model (Fig. S3 a) (7,15). The black line in Fig. 4 B shows the fit for 23°C using parameters listed in Fig. S3 a. T-S curves for 15°C and 40°C were fit by changing a single model parameter, k_0 , which is proportional to the rates of transitions in the channel that accompany ion transit and subsequent resetting of the stator (0.55-fold for 15°C and 2.5-fold for 40°C, blue and red lines, respectively, Fig. 4 B).

Other combinations of parameters were also able to explain the effect of temperature on the T-S curve. For example, an increase in k_1 – k_4 by 12-fold produced a reasonable fit to the T-S curve at 15°C (blue line in Fig. S3 b). However, a change in k_1 – k_4 was not able to produce a good fit at 40°C even by a 1000-fold reduction (dotted orange line in Fig. S3 b) without increasing k_0 by 2.2-fold (red line in Fig. S3 b). This suggests that k_0 is the dominant factor accounting for the effect of temperature. Because the rate of torque generation, k_A , and the reverse rate, k_B , are both proportional to k_0 , the kinetic model suggests that the torque-generating step is temperature sensitive. If we use 7.0×10^{-20} J (19) as the activation free energy, k_0 changes by 0.6-fold upon cooling from 23°C to 15°C, and by 2.6-fold upon heating from 23°C to 40°C. Furthermore, k_A and k_B are estimated to change 0.52- and 0.70-fold during the cooling and 3.58- and 2.01-fold during heating, respectively. Therefore, the torque-generating rate, k_A , appears to be the most temperature-sensitive component of torque generation in this simple treatment of the model. Our result for the Na⁺-driven motor is consistent with the previous report for the H⁺-driven motor suggesting that the rate-limiting step in torque generation is likely to be an elementary step in the proton pathway (6). A possible candidate for the rate-limiting elementary step of H⁺-driven motor may be formation of a hydrogen bond from the protonated MotB Asp-32 to carbonyl-169 of MotA to cause bending of the MotA helix (21).

Torque steps

When temperature was held between 40°C and 50°C, thermal response of the motor was hysteretic. The motor torque at high load was reduced during heating and then recovered during cooling to room temperature in a stepwise manner (Figs. 6 and 7). Torque steps were ~150 pN nm for both falling and recovery phases (Fig. 7). Mean step sizes (173 ± 26 pN nm) did not change over up to 12 heating cycles (Fig. 8 A). Such stepwise changes of torque or speed at high load are signatures of dynamic exchange of stators in and out of a motor (3,22). Stepwise speed change of the chimeric motor can also be induced at a low concentration of external Na⁺ (4). Stators of the motor in *Vibrio alginolyticus* dissociate from the motor at low Na⁺ concentration and reassemble into the motor at high Na⁺ concentration (12). Thus, thermal torque steps most likely reflect stator assembly

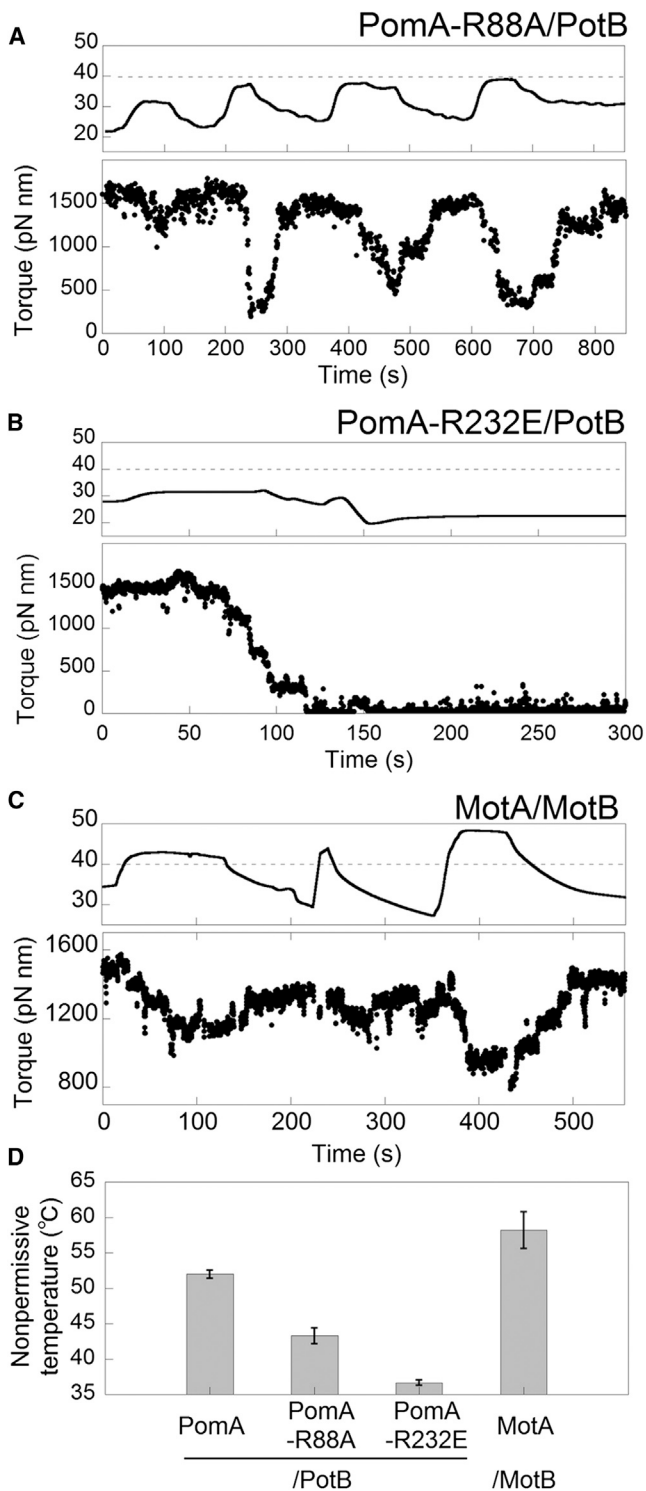


FIGURE 9 Thermal response of PomA mutants and H^+ -driven motor. (A–C) Torque responses of typical PomA-R88A/PotB (A), PomA-R232E/PotB (B), and WT H^+ -driven (MotA/MotB) motors (C) at high load (1.0 μ m beads). Time courses of temperature (top) and torque (bottom) are shown. Heating at 30–40°C for 1–2 min induced reversible torque loss in PomA-R88A/PotB (A). Heating at ~30°C reduced the torque irreversibly in PomA-R232E/PotB in a stepwise manner (B). Heating over 40°C induced reversible torque change in the WT motor (C), as with PomA/PotB. (D) The nonpermissive temperature of the PomA mutants

and H^+ -driven motor. Rotation of tethered cells was observed with a slow increase of temperature (0.027–0.12°C/s). The nonpermissive temperature was measured as the lowest temperature at which no rotating cell was ever observed during the slow temperature increases. The averaged nonpermissive temperature from three experiments is shown, with standard deviation.

Threshold of 40°C

The thermal response of the chimeric motor changed from the nonhysteretic mode to the hysteretic mode above a typical threshold of ~40°C. 40°C seems to be an important temperature for *E. coli* cells, it is reported that leakage at the *E. coli* membrane occurs at >40°C (23). The chimeric motor in *E. coli* showed high thermal tolerance, surviving >10 heating cycles (Fig. 8). At 30–42°C, synthesis of >20 heat shock proteins is induced in *E. coli* (24). Typical temperatures to induce the heat-induced torque change, ~45°C, ~35°C, ~30°C, for PomA, PomA-R88A, PomA-R232E, respectively, are within the temperature range for the induction of these heat shock proteins. Thus, it is interesting to speculate that the thermal tolerance against repeated cycles of heating may be related to the activity of heat shock proteins to supply normally folded stator proteins to the motors.

Sodium motive force

It is reported that motor torque is proportional to ion motive force at high load (25). Ion motive force for the Na^+ -driven motor (*smf*), supplying the energy that drives the torque of the Na^+ -driven motor, can be calculated as

$$smf = e \cdot V_m + kT \cdot \ln \frac{[Na^+]_{in}}{[Na^+]_{out}}, \quad (1)$$

where k is the Boltzmann constant, T is the absolute temperature, e is the fundamental charge of an electron, V_m is membrane voltage, and $[Na^+]_{in}$ and $[Na^+]_{out}$ are the concentrations of sodium ion inside and outside the cell, respectively. $[Na^+]_{out}$ was held at 85 mM in this study. $[Na^+]_{in}$ was previously measured as 14 mM at 23°C (20). We found that V_m is almost constant between 10°C and 40°C (Fig. 5). After the 14–15th heating cycles, unitary torque per stator at room temperature (183 pN nm) (15) was reduced to ~60% (Fig. 8). If this reduction is a consequence of irreversible

reduction in smf , it corresponds V_m falling to $-100 \sim -50$ mV from the previously measured -120 mV with a possible range of $[Na^+]_{in} = 14\text{--}85$ mM. Although changes in smf may be responsible for the behavior after many heating cycles, they appear not to be involved in temperature-dependent stator loss upon heating above 40°C : the constant unitary step size during slowdown and speedup (Figs. 7 and 8) is a strong indicator of unchanging torque per stator and therefore constant smf during temperature-induced stator loss. We attempted to confirm this by measuring the membrane voltage of a single cell during repeated heating cycles above 40°C , but our results were inconsistent and inconclusive. This was most likely due to the lag in voltage response when calculating V_m using dye-equilibration, in comparison with the fast response of motor torque to thermal stress.

Heating over 40°C induced torque steps for the WT H^+ -driven motor (Fig. S4) as well as the Na^+ -driven chimeric motor. Similar torque steps in the chimeric motor were reported in response to loss of smf ; both low $[Na^+]_{out}$ to reduce the concentration gradient (4) and high external pH to reduce V_m (11). Therefore, the H^+ -driven motor and the Na^+ -driven motor may share a mechanism whereby the ion motive force is coupled not only with torque generation but also with the assembly of the motor to maintain the number of active stators. Dissociation of GFP-fused stators from a motor was directly observed for the Na^+ -driven motor in *Vibrio alginolyticus* at low Na^+ concentration (12). Even under normal conditions, dissociation in the fast exchange of single stator protein of WT H^+ -driven motor was observed by total internal reflection fluorescence microscopy (26). Our results show that temperature is also a determinant of stator stability in the motor. Use of these techniques and faster measurement of ion motive force are required to further understand the dynamics of the motor assembly.

PomA mutants as temperature-sensitive mutants

Reduction of motile activity above a threshold temperature and subsequent recovery of motile activity by restoring temperature is typical behavior in temperature-sensitive mutants as reported (8,9), although the mechanism of this thermal response is not known. In the report of Fukuoka et. al., several mutations in PomA at possible sites for the electrostatic interaction with FliG induced temperature-dependent drop and recovery of the swimming fraction of *Vibrio*. In our study, motors with WT amino acid residues at these sites showed hysteresis in thermal responses. This may be due to higher temperatures in this study ($40\text{--}50^\circ\text{C}$) than in the previous reports (42°C), or to the different host species. The R88A mutant showed torque reduction steps at $\sim 10^\circ\text{C}$ lower temperature, consistent with the report that the proposed sites for electrostatic interactions in PomA are important for the thermal response.

Mashimo et. al. reported temperature-sensitive mutants of *Salmonella enterica* serovar Typhimurium with point mutations in rotor proteins (FliG, FliM, and FliN). In these mutants, three point mutations in FliG (F236V, D244Y, and K273E) showed a reversible reduction of the motile fraction of swimming cells in response to transient heating from 20°C to 30°C . Although these three sites are not included in the proposed sites for the electrostatic interaction between MotA-FliG, they may indirectly affect the MotA-FliG interaction, because they are near the proposed site in domain 2 of FliG. Therefore, reversible response of the motor to transient temperature change seems to be related to the proposed electrostatic interaction between stator and rotor. In the report of Mashimo and collaborators, most of the temperature-sensitive mutants, except the three previous mutants, did not recover their motility after restoring temperature. Point mutations at various sites in FliG, FliM, and FliN induced several phenotypes that irreversibly affected motility via a defect of protein transport that resulted in short hooks, a defect in torque generation, or a defect in the switching of rotation. Thus, the irreversible thermal response corresponds to various changes in protein structure and/or their interaction. Point mutation PomA-R232E in this study showed an irreversible thermal response; the threshold temperature of PomA-R232E was further reduced (Fig. 9 B) and the recovery torque of PomA-R232E was barely observable in contrast to the repeated response of PomA-R88A and PomA (Fig. 9 A, Fig. 6). Nevertheless, PomA-R232E also showed stepwise torque in the falling phase (Fig. S5, C and D), which indicated that stators were irreversibly, inactivated one after another.

CONCLUSION

Na^+ -driven chimeric motor expressed in *E. coli* cells showed the nonhysteretic thermal responses up to 40°C with almost constant membrane voltage and torque at high load. By the transient heating above a typical threshold of $\sim 40^\circ\text{C}$, the thermal response changed to the hysteretic mode, showing stepwise reduction in torque upon heating and subsequent recovery upon cooling. A unitary torque step of ~ 150 pN nm suggests the temperature-dependent assembly of stators. Because the thermal torque steps were also observed for the temperature-sensitive mutants (with lower threshold temperatures) and the WT H^+ -driven motor, the temperature-dependent assembly of stators is a general feature of flagellar motors.

SUPPORTING MATERIAL

Five figures, twenty equations, and two methods are available at [http://www.biophysj.org/biophysj/supplemental/S0006-3495\(13\)01251-4](http://www.biophysj.org/biophysj/supplemental/S0006-3495(13)01251-4).

This research was supported by CREST from JST (A.I.); KAKENHI on Innovative Areas from MEXT/JSPS (A.I.); KAKENHI from MEXT/JSPS (A.I. and Y.I.); and FIRST program from JSPS (A.I. and Y.I.). This research was also supported in part by the Management Expenses Grants for National Universities Corporations from MEXT.

REFERENCES

- Sowa, Y., and R. M. Berry. 2008. Bacterial flagellar motor. *Q. Rev. Biophys.* 41:103–132.
- Asai, Y., I. Kawagishi, ..., M. Homma. 1999. Hybrid motor with H⁺- and Na⁺-driven components can rotate *Vibrio* polar flagella by using sodium ions. *J. Bacteriol.* 181:6332–6338.
- Reid, S. W., M. C. Leake, ..., R. M. Berry. 2006. The maximum number of torque-generating units in the flagellar motor of *Escherichia coli* is at least 11. *Proc. Natl. Acad. Sci. USA.* 103:8066–8071.
- Sowa, Y., A. D. Rowe, ..., R. M. Berry. 2005. Direct observation of steps in rotation of the bacterial flagellar motor. *Nature.* 437:916–919.
- Chen, X., and H. C. Berg. 2000. Torque-speed relationship of the flagellar rotary motor of *Escherichia coli*. *Biophys. J.* 78:1036–1041.
- Yuan, J., and H. C. Berg. 2010. Thermal and solvent-isotope effects on the flagellar rotary motor near zero load. *Biophys. J.* 98:2121–2126.
- Sowa, Y., H. Hotta, ..., A. Ishijima. 2003. Torque-speed relationship of the Na⁺-driven flagellar motor of *Vibrio alginolyticus*. *J. Mol. Biol.* 327:1043–1051.
- Fukuoka, H., T. Yakushi, and M. Homma. 2004. Concerted effects of amino acid substitutions in conserved charged residues and other residues in the cytoplasmic domain of PomA, a stator component of Na⁺-driven flagella. *J. Bacteriol.* 186:6749–6758.
- Mashimo, T., M. Hashimoto, ..., S. Aizawa. 2007. Temperature-hypersensitive sites of the flagellar switch component FliG in *Salmonella enterica* serovar typhimurium. *J. Bacteriol.* 189:5153–5160.
- Zhou, J., S. A. Lloyd, and D. F. Blair. 1998. Electrostatic interactions between rotor and stator in the bacterial flagellar motor. *Proc. Natl. Acad. Sci. USA.* 95:6436–6441.
- Lo, C. J., M. C. Leake, ..., R. M. Berry. 2007. Nonequivalence of membrane voltage and ion-gradient as driving forces for the bacterial flagellar motor at low load. *Biophys. J.* 93:294–302.
- Fukuoka, H., T. Wada, ..., M. Homma. 2009. Sodium-dependent dynamic assembly of membrane complexes in sodium-driven flagellar motors. *Mol. Microbiol.* 71:825–835.
- Tipping, M. J., B. C. Steel, ..., J. P. Armitage. 2013. Quantification of flagellar motor stator dynamics through in vivo proton-motive force control. *Mol. Microbiol.* 87:338–347.
- Baker, M. A., Y. Inoue, ..., R. M. Berry. 2011. Two methods of temperature control for single-molecule measurements. *Eur. Biophys. J.* 40:651–660.
- Inoue, Y., C. J. Lo, ..., A. Ishijima. 2008. Torque-speed relationships of Na⁺-driven chimeric flagellar motors in *Escherichia coli*. *J. Mol. Biol.* 376:1251–1259.
- Terasawa, S., H. Fukuoka, ..., A. Ishijima. 2011. Coordinated reversal of flagellar motors on a single *Escherichia coli* cell. *Biophys. J.* 100:2193–2200.
- Nishiyama, S., S. Ohno, ..., I. Kawagishi. 2010. Thermosensing function of the *Escherichia coli* redox sensor Aer. *J. Bacteriol.* 192:1740–1743.
- Kersemakers, J. W., E. L. Munteanu, ..., M. Dogterom. 2006. Assembly dynamics of microtubules at molecular resolution. *Nature.* 442:709–712.
- Iwazawa, J., Y. Imae, and S. Kobayashi. 1993. Study of the torque of the bacterial flagellar motor using a rotating electric field. *Biophys. J.* 64:925–933.
- Lo, C. J., M. C. Leake, and R. M. Berry. 2006. Fluorescence measurement of intracellular sodium concentration in single *Escherichia coli* cells. *Biophys. J.* 90:357–365.
- Kim, E. A., M. Price-Carter, ..., D. F. Blair. 2008. Membrane segment organization in the stator complex of the flagellar motor: implications for proton flow and proton-induced conformational change. *Biochemistry.* 47:11332–11339.
- Ryu, W. S., R. M. Berry, and H. C. Berg. 2000. Torque-generating units of the flagellar motor of *Escherichia coli* have a high duty ratio. *Nature.* 403:444–447.
- Russell, A. D., and D. Harries. 1967. Some aspects of thermal injury in *Escherichia coli*. *Appl. Microbiol.* 15:407–410.
- Arsène, F., T. Tomoyasu, and B. Bukau. 2000. The heat shock response of *Escherichia coli*. *Int. J. Food Microbiol.* 55:3–9.
- Fung, D. C., and H. C. Berg. 1995. Powering the flagellar motor of *Escherichia coli* with an external voltage source. *Nature.* 375:809–812.
- Leake, M. C., J. H. Chandler, ..., J. P. Armitage. 2006. Stoichiometry and turnover in single, functioning membrane protein complexes. *Nature.* 443:355–358.